Lab on a Chip

Cite this: *Lab Chip*, 2011, **11**, 2604

www.rsc.org/loc

PAPER

Asynchronous magnetic bead rotation (AMBR) biosensor in microfluidic droplets for rapid bacterial growth and susceptibility measurements†

Irene Sinn,[abc] Paivo Kinnunen,[ad] Theodore Albertson,[a] Brandon H. McNaughton,[abd] Duane W. Newton,[e] Mark A. Burns[c] and Raoul Kopelman*[abd]

Received 31st December 2010, Accepted 21st April 2011
DOI: 10.1039/c0lc00734j

Inappropriate antibiotic use is a major factor contributing to the emergence and spread of antimicrobial resistance. The long turnaround time (over 24 hours) required for clinical antimicrobial susceptibility testing (AST) often results in patients being prescribed empiric therapies, which may be inadequate, inappropriate, or overly broad-spectrum. A reduction in the AST time may enable more appropriate therapies to be prescribed earlier. Here we report on a new diagnostic asynchronous magnetic bead rotation (AMBR) biosensor droplet microfluidic platform that enables single cell and small cell population growth measurements for applications aimed at rapid AST. We demonstrate the ability to rapidly measure bacterial growth, susceptibility, and the minimum inhibitory concentration (MIC) of a small uropathogenic *Escherichia coli* population that was confined in microfluidic droplets and exposed to concentrations above and below the MIC of gentamicin. Growth was observed below the MIC, and no growth was observed above the MIC. A 52% change in the sensor signal (*i.e.* rotational period) was observed within 15 minutes, thus allowing AST measurements to be performed potentially within minutes.

Introduction

The emergence and spread of antibiotic resistance is a global health concern, as pathogenic species increasingly adapt to antimicrobial agents and classes.[1] Standard antimicrobial susceptibility testing (AST) protocols typically take over 24 hours for a full analysis; as a result, patients are often prescribed empiric therapies prior to diagnosis.[2] Incorrect empiric therapies, such as the inadequate, inappropriate, or overly broad-spectrum use of antimicrobial agents,[3] result in poor patient response and contribute to the increase in multi-drug resistant pathogens. Decreasing the use of unnecessary antibiotics and treating patients with narrow-spectrum agents will help confront this global problem.[3] One approach towards this goal is through the development of rapid AST for earlier diagnosis. Earlier diagnosis will enable more appropriate therapies to be prescribed,[4,5] reduce antibiotic use,[4] and may lead to more effective treatments.[6,7] Subsequently, early diagnosis will reduce health care costs, length of hospital stays, and the spread of antimicrobial resistance.[5]

Traditional methods of microbial identification and differentiation of the infectious organisms rely on phenotypic characteristics, such as morphology and growth. However, molecular diagnostic techniques are increasingly used as adjuncts in clinical AST.[8] These diagnostic techniques, in particular the polymerase chain reaction (PCR), enable rapid detection of pathogen-derived nucleic acids in clinical specimens, thereby reducing identification and diagnosis to a few hours.[9] However, molecular methods are typically more expensive than phenotype-based assays; genetically identical bacteria may exhibit phenotypic heterogeneity potentially leading to inappropriate treatments,[10] and only a few resistance genes have been firmly associated with phenotypic resistance.[11] Ultimately, phenotype-based methods, specifically those that determine the minimum inhibitory concentration (MIC) of the infectious organism, remain the 'gold standard' for clinical AST.[12] Currently, rapid clinical AST measurement tools utilize the growth-based microdilution technique (incorporated by the various commercially available AST systems) to determine the MIC, which is defined as the lowest antibiotic concentration that inhibits visible growth after overnight incubation. Nevertheless, the complete AST protocol, from pathogen isolation to MIC determination, takes well over

[a]*Department of Chemistry, University of Michigan, 930 North University, Ann Arbor, MI, 48109-1055, USA. E-mail: kopelman@umich.edu; Fax: +1 734 936-2778; Tel: +1 734 764-7541*
[b]*Department of Biomedical Engineering, University of Michigan, 2200 Bonisteel, Ann Arbor, MI, 48109-2099, USA*
[c]*Department of Chemical Engineering, University of Michigan, 2300 Hayward Street, Ann Arbor, MI, 48109-2136, USA*
[d]*Applied Physics Program, University of Michigan, 2477 Randall Laboratory, Ann Arbor, MI, 48109-1120, USA*
[e]*Department of Pathology, University of Michigan, Medical School, 1301 Catherine, Ann Arbor, MI, 48109-0602, USA*
† Electronic supplementary information (ESI) available. See DOI: 10.1039/c0lc00734j

24 hours due to the combination of the long culture time (18–24 hours) and the AST measurement time (requiring 6–24 hours). Towards the goal of achieving faster AST measurements, there is a need for the improvement of optical detection methods and/or the development of new approaches to detect microbial proliferation.[11,13]

Microfluidic technologies have been used to reduce the turn-around time for AST, specifically in determining the MIC for infectious bacterial populations. By confining single or small cell populations of bacteria in nanolitre volume droplets, the effective concentration of cells in a system increases.[14] Furthermore, droplet systems are not subjected to dilution effects that are apparent in bulk systems; as a result, cellular biochemical signals or reaction products accumulate in the droplet more rapidly.[14] Using a microfluidic droplet system, the MIC values for *Staphylococcus aureus* cells that were exposed to antibiotics were obtained within 7 hours by measuring the accumulation of a fluorescence viability indicator.[14] Another microfluidic approach confines cells in gas-permeable microchannels with high surface-to-volume ratios, which increases oxygen diffusion into the system.[2] Increased levels of oxygen available to the cells resulted in faster replication rates, and bacterial cells accumulated in the channels more rapidly.[2] *Escherichia coli* bacteria exposed to antibiotics were cultivated in these high surface-to-volume microfluidic channels, allowing AST measurements based on the turbidity of the sample to be obtained within 2 hours from the start of cultivation.[2]

Asynchronous magnetic bead rotation (AMBR) is a recently developed technique that has found many applications as biosensors, specifically in bacterial cell and analyte detection.[15,16] These AMBR biosensors are based on the concept that a magnetic bead that is placed within an external rotating magnetic field has a unique rotational frequency; changes in this magnetic bead's physical properties (*i.e.* shape and volume), or changes in its environment (*i.e.* viscosity), result in detectable changes in the bead's rotational rate.[17] For instance, a bare magnetic bead within a rotating magnetic field has a unique rotational rate; when bacteria bind to the bead, the increased volume of the bead complex results in a decrease in the rotational rate of the bead.[15] Similarly, a modified form of the described method, known as label-acquired-magnetorotation (LAM), was used to measure the analyte concentration in solution by measuring the bead's rotational rate.[16] However, as experiments were conducted under bulk experimental conditions, the AMBR biosensors were subjected to bead translation and magnetic particle-to-particle interactions; as a result, the sensors were actively monitored and tracked, and solutions were highly diluted. Furthermore, the AMBR biosensors were limited to relatively short-term studies because the AMBR biosensor was sensitive to time-dependent effects that were caused by particle–surface adhesion and stiction effects,[17] both of which may reduce the efficiency or accuracy of the sensing system.

Here we report on a new microfluidic diagnostic sensor platform in which individual AMBR biosensors are confined within nanolitre-sized water-in-oil (w/o) droplets for rapid antimicrobial susceptibility testing. Individual AMBR sensors in microfluidic droplets are suspended within a defined space, which allows for easy handling and more efficient measurements, and enables long-duration experiments, such as growth studies, as the beads are separated from the channel walls by a thin oil layer. In addition, enclosing AMBR biosensors in microfluidic droplets allows for the future extension of this platform towards a large-scale, parallel analysis system. For instance, a large array of AMBR sensors that are compartmentalized in droplets of unique chemical, biological, or physical conditions can be monitored continuously over long time-scales.

We apply the AMBR biosensor droplet microfluidic platform for monitoring the growth of bacterial cells at the single cell and small cell-population level and measure bacterial susceptibility to antibiotics. *E. coli* cells that are attached to magnetic beads were encapsulated in microfluidic droplets, and their rotations were monitored through time; as the viable cells grew, the bead's rotational rate consequently decreased. At the single cell level, heterogeneity studies or single cell kinetics studies become possible due to the high sensitivity of the system.[19] Moreover, for clinical AST testing, the collective cellular behavior is of interest, since cells act in a cooperative manner to provide protection, improve survival against competitors[20] and initiate quorum sensing.[21] We extend and apply this AMBR biosensor droplet microfluidic platform towards rapid AST, demonstrate its ability to measure bacterial growth response to antibiotics and determine the MIC value. Towards this end, the AMBR droplet microfluidic platform described here, when used at the small cell-population level, enables rapid measurement of changes in bacterial cell growth in response to external factors. In particular, this system enables the growth response to gentamicin, an aminoglycoside antibiotic, for uropathogenic *E. coli* cells to be detectable within 15 minutes, as shown below.

Materials and methods

Materials and reagents

The following materials and reagents were used. PCR grade mineral Oil, Span® 80, and Bovine Serum Albumin (BSA) were purchased from Sigma-Aldrich Corp (St Louis MO). Dulbecco-PBS was purchased from Invitrogen (Carlsbad CA). Mueller Hinton II (MH Broth) was purchased from Teknova (Hollister CA). Dispense tips, syringe barrels, and a barrel adapter kit were purchased from Nordson, EFD (East Providence, RI). Pluronic F-68 was purchased from MP Biochemicals (Santa Ana, CA). The Tygon Silicon Tubing (02-587-1D) was purchased from Saint-Gobain Performance Plastics (Aurora OH). Inlet/Outlet adapters were purchased from Small Parts Inc. (St Logansport IN). The 8.8 μm streptavidin-coated superparamagnetic beads (8.8 ± 0.8 μm) were purchased from Spherotech, Inc. (Lake Forest IL), and Dynabead® M-280 Streptavidin-coated superparamagnetic beads (2.8 ± 0.2 μm) were purchased from Invitrogen (Carlsbad CA).

The continuous phase consisted of mineral oil with 1% Span® 80 (v/v). For bead characterization experiments, the aqueous phase consisted of PBS solution: PBS with 1% Pluronic F-68 and 0.1% BSA. For biological experiments, the aqueous phase consisted of MH broth solution: MH with 1% Pluronic F-68 and 0.1% BSA, which will be referred to as MH-PB.

Device fabrication

Channel geometries were designed with LEdit. The procedure for the fabrication process, including the photolithography and wet chemical etching steps, on a glass wafer is detailed elsewhere.[22] Briefly, 50 nm Cr and 250 nm Au were deposited onto a 4″ borosilicate glass wafer (Precision Glass & Optics, Santa Ana CA). The wafer was patterned and the glass channels were etched in CMOS grade hydrofluoric acid (49%) (J. T. Baker, Philipsburg, NJ) to a depth between 45 μm and 50 μm, as measured with a surface profilometer. The photoresist and metal layers were removed, the glass wafer diced to obtain individual devices, and inlet and outlet holes were electrochemically drilled. The devices were cleaned in Piranha solution (2 : 1 solution of sulfuric acid and hydrogen peroxide, respectively) and subsequently coated with a 2 μm layer of Parylene-C (PDS 1020 Labcoater, Specialty Coating Systems, Indianapolis, IN). The devices were UV-glued to a standard No. 0 cover glass slide (Goldseal cover glass Thickness #0 260320; Tedpella, Redding, CA), and inlet and outlet ports were UV-glued to the device. A simplified schematic of the fabrication process is outlined in Fig. 1(a), and the assembled glass microfluidic droplet device is shown in Fig. 1(b).

Experimental setup and operation

Experiments were conducted on an Olympus IX71 inverted microscope. The microfluidic device was placed inside custom-built electromagnet coils that were integrated on the microscope stage [Fig. 1(c)]. The rotating magnetic field was generated with a custom LabView (National Instruments, Austin, TX) program and data acquisition board (NI PCI-6221; National Instruments, Austin, TX). The magnetic field driving frequency range was 0.1 Hz to 1 kHz, and the magnetic field strength at the region of interest, *e.g.* microchannel, was 0.9 mT, as measured with a 3-axis magnetic field probe (C-H3A-2m; Senis GmbH, Switzerland).

Bead characterization experiments and the preliminary experiments for the single cell growth measurements were conducted at room temperature (21 ± 2 °C), with a 100× oil immersion objective. The magnetic field driving frequency was set at 500 Hz for control and growth experiments. One-minute videos at 15 frames per second (fps) were taken in 5 minute intervals with a digital camera. Small cell-population experiments were conducted at near physiological temperatures, 35 ± 0.2 °C, with a 40× objective. The microfluidic device was placed on an ITO slide (SPI Supplies, West Chester, PA) that was heated from room temperature and maintained at a set temperature, 35 ± 0.2 °C. This temperature was monitored by a thermocouple that was coupled to the surface of the slide with a thermally conducting silver paste, Arctic Silver 5 (Arctic Silver Incorporated, Visalia, CA). The magnetic field driving frequency for small cell-population control and growth experiments was set at 50 Hz, and continuous 2 fps videos were taken for a minimum of 5 hours. For small cell-population control and antibiotic response experiments, 1 minute videos were taken at 20 fps in either 5 minute or 20 minute intervals.

Data acquisition and analysis

Movies were captured with a digital camera (piA640-210gm; Basler Inc., Exton, PA). The videos were analyzed using ImageJ—see Fig. 1(d). The rotational frequency of the bead complex was determined by monitoring the fluctuations in intensity profile at the target area of interest using ImageJ's 'plot *z*-axis profile' functionality. This intensity plot was analyzed by applying a Fast Fourier Transform (FFT) to the raw ImageJ data in MATLAB. The experimental error in determining the rotational period was designated as the FFT peak's full width at half max (FWHM) of the amplitude signal.[23]

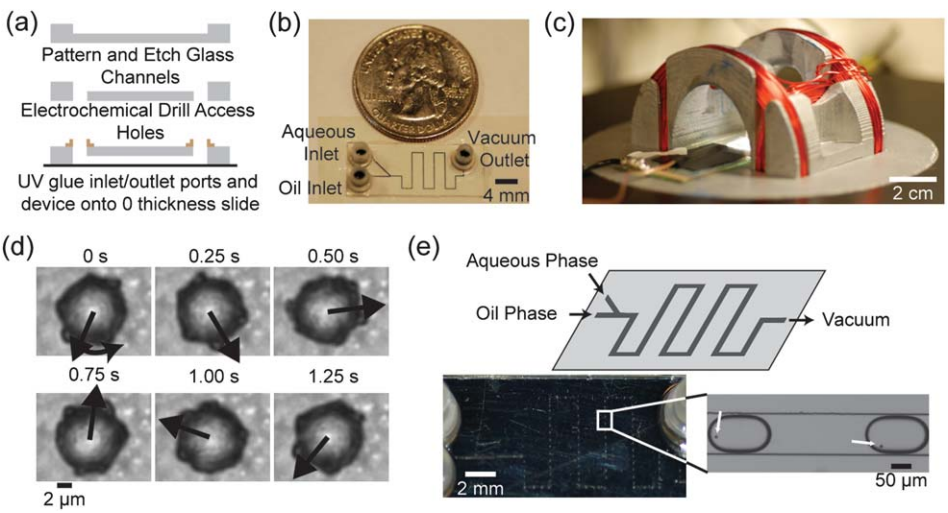

Fig. 1 (a) Microfluidic glass channels were patterned and etched using standard glass lithography. (b) Image of the microfluidic droplet device. (c) A picture of the microfluidic device inside the electromagnet coils, which generate a rotating magnetic field at its core. (d) Optical microscopy image of an 8.8 μm magnetic bead rotating asynchronously with an external rotating magnetic field at a 50 Hz driving frequency, bead rotation rate being much lower (0.8 Hz). Visual aid is provided to observe the bead rotation. (e) Droplets of 0.5 nL to 1 nL in volume were formed by applying a vacuum at the outlet and applying hydrostatic pressure at the oil inlet. A microfluidic device of this design holds between 50 and 75 droplets.

Droplet formation

To further increase channel hydrophobicity, the channels were treated with Rain-X® Original Glass Treatment (SOPUS Products, Houston, TX) prior to experiments; 10 μL of Rain-X was pipetted into the outlet reservoir, and the channel's inherent hydrophobicity resulted in the solution rapidly filling the channels. The Rain-X solution was allowed to stay in the devices for 10 minutes, after which vacuum was applied at the outlet by a vacuum pump (Rocker 300; Lab Depot Inc., Dawsonville, GA) until the channels were replaced by air. Then, the continuous phase (mineral oil) and 10 μL of aqueous phase were introduced at their respective inlet reservoirs; the continuous phase wetted the channel walls and fully entered the channels. The hydrostatic pressure applied at the inlet of the continuous phase was controlled by adjusting the pressure at the inlet, *i.e.* the height of the oil reservoir. To create droplets of approximately 0.5–1 nL in volume—see Fig. 1(e), the vacuum strength was set between 70 kPa and 90 kPa and the hydrostatic pressure of the continuous phase was set between 1.2 kPa and 1.9 kPa.

Bacteria growth in droplets

The streptavidin coated M-280s and 8.8 μm magnetic beads were incubated with biotinylated anti-*E. coli* (ab20640-1; Abcam Cambridge UK) at 37 °C for 2 hours on a shaking platform at 175 rpm. A uropathogenic clinical *E. coli* isolate was grown on Muller-Hinton agar plates (BD Diagnostic Systems, Franklin Lakes, NJ) at 37 °C for 16 to 18 hours. A 2 mL vial of MH broth was inoculated with bacteria to a 0.5 McFarland standard (approximately 1.5×10^8 CFU mL^{-1}). Anti *E. coli* functionalized magnetic beads, M-280 beads for single-cell growth experiments and 8.8 μm magnetic beads for small cell-population growth experiments were introduced to the bacteria solution, and the sample was incubated at 37 °C for 1.5 hours in a 1.5 mL microcentrifuge tube on a shaking platform at 175 rpm. This allowed the bacteria to bind to the beads and enter the exponential phase. The bacteria-bound beads were isolated with a magnetic separator (PickPen 1-M; Sunrise Science Products, San Diego, CA), washed in MH broth twice and re-suspended into MH-PB.

For experiments in which bacteria were fixed with glutaraldehyde, an MH broth solution with 0.5% glutaraldehyde was used. Bacteria-bound beads were isolated with a magnetic separator, washed twice and re-suspended into MH-PB with 0.5% glutaraldehyde solution (Sigma-Aldrich, St Louis, MO).

Bacterial antibiotic response

Gentamicin solution (Sigma-Aldrich, St Louis MO) serial dilutions were prepared in MH-PB broth at concentrations of 4, 16, and 32 μg mL^{-1}, and aliquots were stored refrigerated at 4 °C. Before each experiment, the antibiotic solution was diluted to their final concentrations of 0.5, 2, and 4 μg mL^{-1}, respectively, by adding 350 μL MH broth experimental solution to the 50 μg mL^{-1} of the initial gentamicin aliquot solutions. The bacteria-bound beads were isolated with a magnetic separator, washed twice, and re-suspended into the antibiotic solution. Experiments started within 20 minutes of antibiotic exposure.

Clinical VITEK®2 testing

Reference MIC values were measured for the uropathogenic *E. coli* isolate using the VITEK 2 XL (bioMérieux, Inc., Durham, NC) automated antimicrobial susceptibility testing platform in a clinical setting.

Results and discussion

Device characterization

Compartmentalizing single magnetic beads in water droplets suspended in oil reduced bead-to-bead magnetic interaction effects, bead-to-surface interaction effects, and prevented the bead from translating out of the field-of-view. The applied vacuum pressure at the outlet and the applied pressure at the inlets determined the resultant droplet size. For the following experiments, the droplets ranged from 0.5 to 1 nL in volume. The current device design accommodated between 50 and 70 droplets [Fig. 1(e)]. For single magnetic bead experiments, we maximized the number of droplets containing a single magnetic bead; the encapsulation process follows Poisson statistics, which can be expressed by $f(\lambda, n) = \frac{\lambda^n e^{-\lambda}}{n!}$, where $f(\lambda,n)$ is the frequency of observing a droplet containing n beads at a given λ value, and λ is

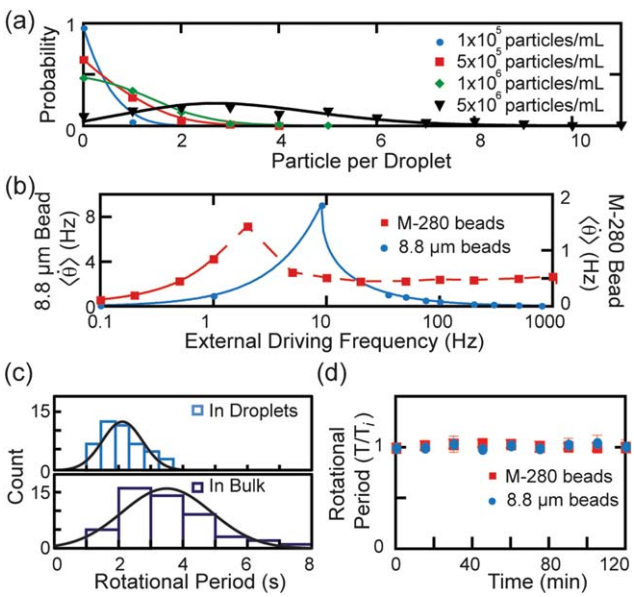

Fig. 2 (a) The frequency of the number of beads per droplet with various particle concentrations. The data are fitted to the Poisson model. (b) Frequency-dependent rotational response curves at driving frequencies between 0.1 Hz and 1000 Hz. The solid line represents the rotational response dominated by a permanent dipole; the dashed lines connect the data to aid in visualization. (c) Rotational response of fifty 8.8 μm beads in 50 Hz driving field in droplets (top) and on glass surface (bottom) with 10^6 beads per mL concentration. The rotational period for beads in droplets was calculated to be 2.11 ± 0.62 s, providing a coefficient of variation of 30%. The beads on glass surface are subject to magnetic and surface interactions; as a result, the average rotational period was 3.5 ± 1.4 s (40% CV). The data are fitted to the normal distribution. (d) Normalized rotational response of 8.8 μm magnetic beads at a driving frequency of 50 Hz for 120 minutes under constant environmental conditions.

the expected average number of beads per droplet (*e.g.* $\lambda = 1$, if 1 mL droplets were formed from an aqueous solution at a concentration 1 bead per mL). Droplets were formed from aqueous solution of 8.8 μm bead at the following concentrations: 1×10^5, 5×10^5, 1×10^6, and 5×10^6 beads per mL, and the number of beads observed in each droplet was counted. The data were fitted with the Poisson distribution, and the corresponding Lambda values were found to be 0.043, 0.43, 0.75, and 3.2 [Fig. 2 (a)]. Using an initial concentration of 1×10^6 beads per mL ($\lambda = 0.75$), we obtained single beads in 35% of the droplets formed.

The frequency-dependent rotational responses of the 8.8 μm and M-280 magnetic beads isolated in individual droplets were characterized with AMBR at driving frequencies between 0.1 Hz and 1 kHz. The rotational behavior of the 8.8 μm beads was dominated by its permanent dipole for frequencies up to 1 kHz, whereas the rotational behavior of the M-280 beads was dominated by its permanent dipole at frequencies below 10 Hz and by its induced dipole above 10 Hz [Fig. 2(b)]. The rotational responses of fifty plain 8.8 μm magnetic beads were observed at 50 Hz driving frequency [see Fig. 2(c)], and the average rotational period was determined to be 2.12 ± 0.62 s, resulting in a magnetic responsiveness variability of 30%. Similar variability in magnetic responsiveness has been reported previously.[24]

Under controlled environmental conditions, the rotational rate of a magnetic bead is expected to be time-independent. The rotational periods for single 8.8 μm beads and single M-280 beads were monitored for 2 hours. The rotational response varied by 5% for the 8.8 μm beads and by 3% for the M-280 beads, as shown in Fig. 2(d). The sensitivity of the system was taken to be the minimum effective volumetric change needed to observe a change in the bead's rotational response (greater than the 5% experimental error observed for the 8.8 μm beads and the 3% experimental error observed for the M-280 beads, see above), corresponding to 0.09 μm sensitivity for 8.8 μm beads, and 0.03 μm sensitivity for the M-280 beads. Since the bead sensitivity was largely dependent on the initial bead diameter, the size choice of the magnetic bead is application dependent.[23]

Theory of magnetic bead rotation

The rotational response of a magnetic bead, when placed within an external rotational magnetic field, is frequency dependent and is governed by its permanent or induced magnetic dipole. A magnetic bead with a permanent magnetic dipole, in a rotating magnetic field with a frequency of Ω, will have an average rotational frequency of $\langle\dot{\theta}\rangle = \Omega$, when $\Omega < \Omega_c$, and $\langle\dot{\theta}\rangle = \Omega - \sqrt{\Omega^2 - \Omega_c^2}$, when $\Omega > \Omega_c$, where the critical frequency $\Omega_c = mB/\kappa\eta V_H$,[17,25] where m is the bead's magnetic moment, B is the magnetic field amplitude, κ is the shape factor (6 for a sphere), η is the dynamic viscosity, and V_H is the hydrodynamic volume of the rotating body.[17,25,26] When $\Omega > \Omega_c$, information about the magnetic bead complex or the external environment can be calculated by observing its rotation rate.[27] For experimental conditions in which m, B, and η are constants, Ω_c is inversely proportional to κ and V_H, which we define as the effective volume, $V_{eff} = \kappa V_H$, as shown by:

$$\langle\dot{\theta}\rangle = \Omega - \sqrt{\Omega^2 - (A/V_{eff})^2}, \quad (1)$$

where $A = mB/\eta$ is a constant.

For magnetic beads with an induced dipole, the bead's rotational frequency is $\dot{\theta} = (\chi'' B^2 V_m)/(\mu_0 \eta \kappa V_H)$, where χ'' is the imaginary susceptibility of the bead, V_m is the volume of the magnetic content of the bead, and μ_0 is the permeability of free space.[19,28] For experimental conditions in which η, B, χ'', μ_0, and V_m are constants, the rotational rate of the bead is expressed by:

$$\dot{\theta} \propto \frac{1}{\kappa V_H} \propto \frac{1}{V_{eff}}. \quad (2)$$

In summary, the changes in the effective volume for beads can be observed by measuring changes in the rotational rate for particles with either a permanent or induced magnetic dipole.

Single bacterium growth measured with AMBR

Monitoring single cell growth with high sensitivity without the influence from neighboring cells is of interest in scientific and clinical applications such as cell heterogeneity,[10,29] bacterial persistence[10] and cellular kinetics. M-280 magnetic beads were used to monitor single bacterium growth and division events, as smaller beads are more sensitive to monitoring smaller cell volumetric changes. The average size of an *E. coli* bacterium is 2 μm in length and 0.5 μm in diameter, which is comparable in size with a M-280 magnetic bead. In this system, nanometre growth was detectable by measuring changes in the bead's rotational response.[19]

The schematic of the growth and division process for a single bacterium at room temperature (21 ± 2 °C) is presented in Fig. 3 (a). The corresponding changes observed with light microscopy and rotational response measurements are shown in Fig. 3(b) and (c), and are in good agreement. Since the effective volume is dependent on the shape factor and the volume of the rotating body (AMBR biosensor), the time at which a substantial change can be observed depends largely on the orientation of the bacteria on the bead. For the case in which the bacterium was bound at one end and grew perpendicularly to the magnetic bead [Fig. 3(a) and (b)], a 17 ± 1% change in the rotational period was observed within 5 minutes [Fig. 3(c)], which is above the experimental error of 3%. From the time at which the rotational rate was first monitored until the time at which the bacterium divided (103 min), the rotational period increased by 400%.

The substantial drop in rotational period (reduction in the sensors effective volume) that was observed at 103 minutes corresponded with bacterial division. As a control, a single bacterium that was attached to a magnetic bead was fixed with glutaraldehyde and the rotational response was measured. No substantial change in the bead's rotational period was observed in 2 hours, which indicated a lack of growth [Fig. 3(c)]. As a result, we concluded that the observed changes in the rotational period of the AMBR sensor were indeed due to the growth, or elongation, of a single bacterial cell. These findings correspond well with a previous study on single cell growth with AMBR biosensors.[19]

Small cell-population growth measured with AMBR

To monitor small cell-population growth, 8.8 μm magnetic beads were used since the larger surface area provided greater binding

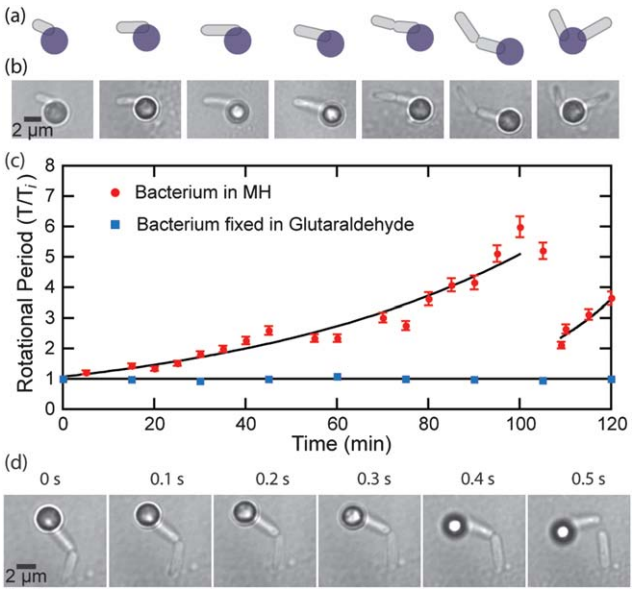

Fig. 3 Single cell growth measurements using the AMBR sensor. (a) A schematic representation of bacterial growth and division at select time points, which corresponds to (b) light microscopy images of bacterial growth and division. (c) The rotational period of the bead and bacteria complex (AMBR biosensor) shown in (b). At the point of division, at 103 minutes, the rotational period decreases, as the effective volume of the biosensor is substantially reduced. The data, of each bacteria generation, are fitted by an exponential curve. The error bars represent the measurement error. (d) Optical microscopy image sequence of the bacteria division process at time 103 minutes.

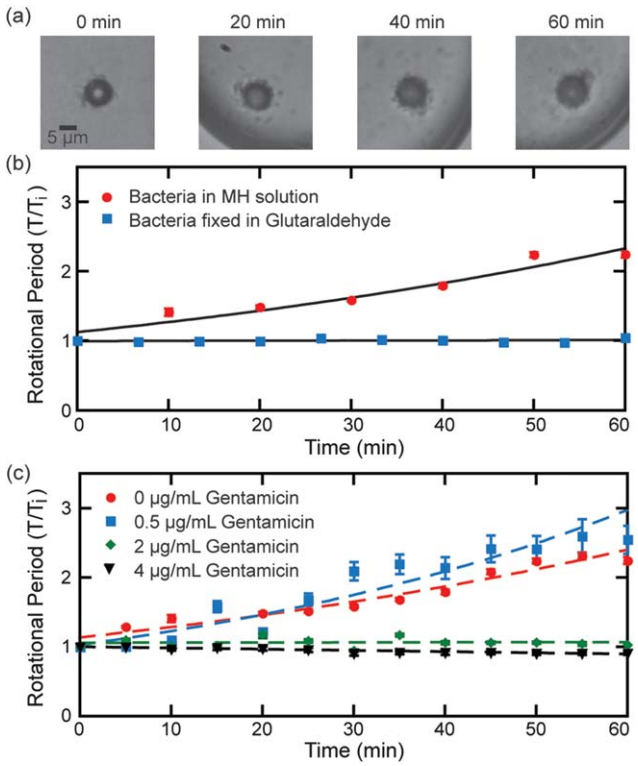

Fig. 4 Small cell-population growth and susceptibility measurements using the AMBR sensor. (a) Optical microscopy images of small cell-population growth on an 8.8 μm magnetic bead in MH-PB solution. (b) The rotational period of the 8.8 μm bead corresponding to the figures above (red circles), and bacteria that have been fixed in glutaraldehyde (blue squares). The data are fitted with an exponential curve. (c) Averaged rotational responses from 3 separate experiments, each of 0 μg mL^{-1} and 0.5 μg mL^{-1} and 2 separate experiments, each of 2 μg mL^{-1} and 4 μg mL^{-1} gentamicin. The MIC, as determined by the VITEK 2 system, is 1 μg mL^{-1}. Bacteria treated with gentamicin concentrations below the MIC continued to grow, whereas bacteria treated with concentrations above the MIC did not show noticeable growth. The difference is evident within 15 min. Datasets are fitted to an exponential curve. The error bars represent the measurement error.

capacity. Experiments were conducted at near physiological conditions, 35 ± 2 °C, and therefore, bacteria replication time was substantially reduced as compared to the single cell growth experiments. The growth of a small population of bacterial cells attached to a bead was measured with AMBR, as shown in Fig. 4 (a). As the bacteria grew and divided, some daughter cells re-attached to the magnetic bead and some remained detached, free-floating in the solution [Fig. 4(a)]. Daughter cells that re-attached to the bead increased the bead's effective volume, which was observed by an increase in the rotational period [Fig. 4(b)]—see ESI† videos. An 8 ± 0.3% average increase in the rotational period was detected after 5 minutes, which is above the 5% experimental error [Fig. 4(a and b)]. As a result, the concentration of bacteria in the liquid environment exponentially increased. To ensure that the initial increase in rotational period was indeed a result of growth, the rotational period was monitored for bacteria-bound beads that were fixed with glutaraldehyde. A 3% variation in rotational period was observed for fixed bacteria, which was consistent with the control experiments for beads without bacteria. Therefore, the measured changes in the rotational period are attributed to bacterial growth.

Small cell-population growth response to gentamicin

The AMBR droplet microfluidic platform was tested with respect to AST applications by measuring the growth response of a small population of uropathogenic *E. coli* towards gentamicin, a bactericidal antibiotic that interrupts protein synthesis. The effects of the antibiotics on the growth of the bacteria could be discerned within an hour. Bacteria bound to 8.8 μm beads were grown in 0, 0.5, 2, and 4 μg mL^{-1} concentrations of gentamicin, and the rotational periods of the beads were monitored for a minimum of one hour. Data for the first 60 minutes are presented in Fig. 4(c). An increase in rotational period was observed for the bacteria cultured in 0 and 0.5 μg mL^{-1} gentamicin, which indicates bacterial growth. No substantial change in the rotational period was observed for the bacteria cultured in 2 and 4 μg mL^{-1} gentamicin, which suggests a lack of growth. The estimated MIC as determined with AMBR is consistent with the MIC value of 1 μg mL^{-1}, as determined with the VITEK 2 system. A 100% difference in the rotational period between bacteria that were treated with gentamicin above and below the MIC was measured within 30 minutes. After only 15 minutes a 52% difference in the rotational period was observed. The rotational trend observed for bacteria treated with gentamicin above the MIC was indeed similar to the results for bacteria fixed with glutaraldehyde. With the presented AMBR microfluidic droplet platform, the effects of

an antibiotic on bacterial growth can be discerned within 30 minutes (15 minutes for sample preparation and 15 minutes for AST measurements). The high sensitivity of this method and the highly parallel nature of microfluidics suggest a promising future potential of this AMBR microfluidic droplet platform sensor towards rapid MIC measurements.

Conclusion

In this paper we demonstrated an AMBR biosensor microfluidic droplet platform that could have significant clinical importance in rapid AST, especially with the incorporation of high-throughput capabilities and portability. Large-scale analysis on single cells and small populations of cells is possible through the use of surfactants that allow droplets to be closely packed[30] or through structures that enable parallel experiments.[21] This will enable the study of cell heterogeneity and behavior at the single cell level and MIC tests to be conducted on the small cell population level. Microfluidic device technologies to study single cells[31,32] or small cell populations exist;[33,34] nevertheless, most phenotype-based systems are limited to direct microscope examination and analysis.[9] Cantilevers provide a non-microscopy, highly sensitive technique to measure growth,[35,36] but these systems require labor-intensive fabrication procedures, in addition to expensive and precisely controlled equipment.

In contrast, the AMBR biosensor platform is a potentially inexpensive, large-scale analysis system. For instance, the AMBR signal can be measured with a low-power laser and a photodiode combination; the light scattered by a rotating magnetic bead can be captured by a photodiode and subsequently analyzed.[37] AMBR biosensors can also be monitored using an inexpensive CMOS pixel array that is placed directly under the microfluidic platform.[38] The CMOS pixel array approach offers a highly parallel method for measuring the signal of multiple AMBR sensors concurrently, provided the magnetic bead is larger in size than a single pixel. Furthermore, optical detection methods may also be replaced with magnetic detection methods, such as magneto-resistive sensors, Hall sensors, or field coils.[18] Although in the present manuscript, the AMBR sensors used to measure bacterial growth were monitored with optical microscopy, continuing development in large-scale AMBR detection methods would eliminate the need for microscope observations in future developments.

In summary, the presented AMBR microfluidic droplet platform enables single cell and small cell-population growth to be rapidly monitored; we demonstrated that this platform could be extended towards application for AST, in measuring MIC values. The droplets provide magnetic and hydrodynamic isolation between AMBR sensors and allow a single sensor to be monitored continuously for hours. Single cell growth and division events and small cell-population growth, in the absence and presence of antibiotics, were detected by measuring changes in the magnetic bead's rotational response; the results were verified with optical microscopy. We functionally characterized a uropathogenic clinical *E. coli* isolate's response to a gentamicin dose within 15 minutes and, based on such measurements on 4 doses, estimated the MIC to be between 0.5 and 2 μg mL^{-1}, a value that is consistent with clinical results. Further development of this platform, such as parallelizing the channels to conduct concurrent measurements on multiple antibiotic concentrations; close-packing the droplets to monitor multiple droplets;[30] and heating the system to physiological temperature, will enable a full AST analysis to be conducted in a single run. This would subsequently reduce the current standard phenotypic AST measurement time (6–24 hours) to within 15–30 minutes.

Acknowledgements

This study was supported by NIH grant R21EB009550 (RK), NSF grant NSF-DMR 9900434 (RK), a Coulter grant (BHM/DN/RK) and a grant from the National Center for Research Resources UL1RR024986 (BHM). BHM and PK disclose financial interest in Life Magnetics, Inc. The authors would also like to acknowledge Alex Hrin for creating the video capture LabVIEW program, the University of Michigan's (UM) Lurie Nanofabrication Facility (LNF), the UM Chemical Engineering Clean Room for use of facilities, chemicals, and fabrication equipment, and the reviewers for their constructive comments.

References

1 J. L. Martinez, A. Fajardo, L. Garmendia, A. Hernandez, J. F. Linares, L. Martínez-Solano and M. B. Sánchez, *FEMS Microbiol. Rev.*, 2009, **33**, 44–65.
2 C. H. Chen, Y. Lu, M. L. Sin, K. E. Mach, D. D. Zhang, V. Gau, J. C. Liao and P. K. Wong, *Anal. Chem.*, 2010, **82**, 1012–1019.
3 B. Schwartz, *Clin. Infect. Dis.*, 1999, **28**, 211–213.
4 J. J. Kerremans, P. Verboom, T. Stijnen, L. Hakkaart-van Roijen, W. Goessens, H. A. Verbrugh and M. C. Vos, *J. Antimicrob. Chemother.*, 2008, **61**, 428–435.
5 J. Barenfanger, C. Drake and G. Kacich, *J. Clin. Microbiol.*, 1999, **37**, 1415–1418.
6 K. Gupta, D. Scholes and W. E. Stamm, *JAMA, J. Am. Med. Assoc.*, 1999, **281**, 736–738.
7 G. V. Doern, R. Vautour, M. Gaudet and B. Levy, *J. Clin. Microbiol.*, 1994, **32**, 1757–1762.
8 E. Goldman and L. H. Green, *Practical Handbook of Microbiology*, CRC Press, 2008.
9 J. Weile and C. Knabbe, *Anal. Bioanal. Chem.*, 2009, **394**, 731–742.
10 N. Q. Balaban, J. Merrin, R. Chait, L. Kowalik and S. Leibler, *Science*, 2004, **305**, 1622–1625.
11 J. H. Jorgensen and M. J. Ferraro, *Clin. Infect. Dis.*, 2009, **49**, 1749–1755.
12 J. M. Andrews, *J. Antimicrob. Chemother.*, 2001, **48**, 5–16.
13 J. H. Jorgensen and M. J. Ferraro, *Clin. Infect. Dis.*, 1998, **26**, 973–980.
14 J. Q. Boedicker, L. Li, T. R. Kline and R. F. Ismagilov, *Lab Chip*, 2008, **8**, 1265–1272.
15 B. H. McNaughton, R. R. Agayan, R. Clarke, R. G. Smith and R. Kopelman, *Appl. Phys. Lett.*, 2007, **91**, 224105.
16 A. Hecht, P. Kinnunen, B. H. McNaughton and R. Kopelman, *J. Magn. Magn. Mater.*, 2010, **323**, 272–278.
17 B. H. McNaughton, K. A. Kehbein, J. N. Anker and R. Kopelman, *J. Phys. Chem. B*, 2006, **110**, 18958–18964.
18 M. A. Gijs, *Microfluid. Nanofluid.*, 2004, **1**, 22–40.
19 P. Kinnunen, I. Sinn, B. H. McNaughton, D. W. Newton, M. A. Burns and R. Kopelman, *Biosens. Bioelectron.*, 2011, **26**, 2751–2755.
20 J. A. Shapiro, *Annu. Rev. Microbiol.*, 1998, **52**, 81–104.
21 D. B. Weibel, W. R. DiLuzio and G. M. Whitesides, *Nat. Rev. Microbiol.*, 2007, **5**, 209–218.
22 R. Pal, M. Yang, R. Lin, B. N. Johnson, N. Srivastava, S. Z. Razzacki, K. J. Chomistek, D. C. Heldsinger, R. M. Haque, V. M. Ugaz, P. K. Thwar, Z. Chen, K. Alfano, M. B. Yim, M. Krishnan, A. O. Fuller, R. G. Larson, D. T. Burke and M. A. Burns, *Lab Chip*, 2005, **5**, 1024–1032.
23 P. Kinnunen, I. Sinn, B. H. McNaughton and R. Kopelman, *Appl. Phys. Lett.*, 2010, **97**, 223701.
24 U. O. Häfeli, M. A. Lobedann, J. Steingroewer, L. R. Moore and J. Riffle, *J. Magn. Magn. Mater.*, 2005, **293**, 224–239.

25 A. Cēbers and M. Ozols, *Phys. Rev. E: Stat., Nonlinear, Soft Matter Phys.*, 2006, **73**, 021505.
26 G. Korneva, H. Ye, Y. Gogotsi, D. Halverson, G. Friedman, J. C. Bradley and K. G. Kornev, *Nano Lett.*, 2005, **5**, 879–884.
27 B. H. McNaughton, R. R. Agayan, J. X. Wang and R. Kopelman, *Sens. Actuators, B*, 2007, **121**, 330–340.
28 X. Janssen, A. Schellekens, K. van Ommering, L. van IJzendoorn and M. Prins, *Biosens. Bioelectron.*, 2009, **24**, 1937–1941.
29 N. Dhar and J. D. McKinney, *Curr. Opin. Microbiol.*, 2007, **10**, 30–38.
30 E. Brouzes, M. Medkova, N. Savenelli, D. Marran, M. Twardowski, J. B. Hutchinson, J. M. Rothberg, D. R. Link, N. Perrimon and M. L. Samuels, *Proc. Natl. Acad. Sci. U. S. A.*, 2009, **106**, 14195–14200.
31 A. R. Wheeler, W. R. Throndset, R. J. Whelan, A. M. Leach, R. N. Zare, Y. H. Liao, K. Farrell, I. D. Manger and A. Daridon, *Anal. Chem.*, 2003, **75**, 3581–3586.
32 D. D. Carlo, L. Y. Wu and L. P. Lee, *Lab Chip*, 2006, **6**, 1445–1449.
33 P. J. Hung, P. J. Lee, P. Sabounchi, N. Aghdam, R. Lin and L. P. Lee, *Lab Chip*, 2005, **5**, 44–48.
34 R. Gómez-Sjöberg, A. A. Leyrat, D. M. Pirone, C. S. Chen and S. R. Quake, *Anal. Chem.*, 2007, **79**, 8557–8563.
35 K. Y. Gfeller, N. Nugaeva and M. Hegner, *Biosens. Bioelectron.*, 2005, **21**, 528–533.
36 M. Godin, F. F. Delgado, S. Son, W. H. Grover, A. K. Bryan, A. Tzur, P. Jorensen, K. Payer, A. D. Grossman, M. W. Kirschner and S. R. Manalis, *Nat. Methods*, 2010, **7**, 387–390.
37 B. H. McNaughton, P. Kinnunen, R. G. Smith, S. Pei, R. Torres-Isea, R. Kopelman and R. Clarke, *J. Magn. Magn. Mater.*, 2009, **321**, 1648–1652.
38 I. Sinn, P. Kinnunen, M. A. Burns, and R. Kopelman, unpublished work.